iScience

CellPress OPEN ACCESS

Article

Strain-controlled synthesis of ultrathin hexagonal $GaTe/MoS_2$ heterostructure for sensitive photodetection

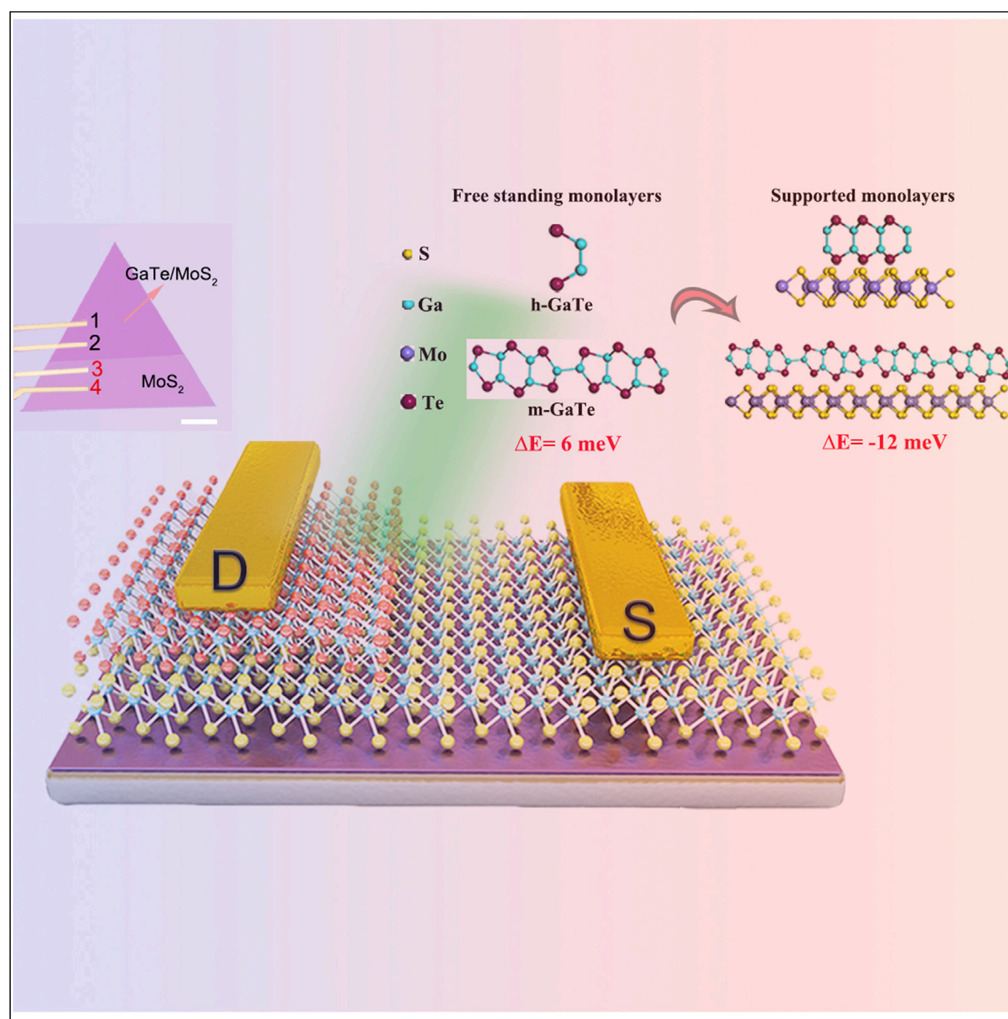

Fang Li, Mingxing Chen, Yajuan Wang, ..., Ziwei Li, Dong Li, Anlian Pan

zhuxiaoli@hnu.edu.cn (X.Z.)
liidong@hu.edu.cn (D.L.)
anlian.pan@hnu.edu.cn (A.P.)

Highlights

High-quality ultrathin hexagonal GaTe is synthesized via strain engineering

Phase transition mechanism of GaTe is revealed by using theoretical calculation

Excellent photosensing properties are observed in $GaTe/MoS_2$ p-n heterostructure

Li et al., iScience *24*, 103031
September 24, 2021 © 2021 The Authors.
https://doi.org/10.1016/j.isci.2021.103031

Check for updates

iScience

CellPress
OPEN ACCESS

Article

Strain-controlled synthesis of ultrathin hexagonal $GaTe/MoS_2$ heterostructure for sensitive photodetection

Fang Li,[1,2,4] Mingxing Chen,[3,4] Yajuan Wang,[1] Xiaoli Zhu,[1,*] Xuehong Zhang,[1] Zixing Zou,[1] Danliang Zhang,[1] Jiali Yi,[1] Ziwei Li,[1] Dong Li,[1,*] and Anlian Pan[1,5,*]

SUMMARY

Ultrathin hexagonal GaTe, with relatively high charge density, holds great potential in the field of optoelectronic devices. However, the thermodynamical stability limits it fabrications as well as applications. Here, by introducing two-dimensional MoS_2 as the substrate, we successfully realized the phase-controlled synthesis of ultrathin h-GaTe, leading to high-quality h-GaTe/MoS_2 heterostructures. Theoretical calculation studies reveal that GaTe with hexagonal phase is more thermodynamically stable on MoS_2 templates, which can be attributed to the strain stretching and the formation energy reduction. Based on the achieved p-n heterostructures, optoelectronic devices are designed and probed, where remarkable photoresponsivity (32.5 A/W) and fast photoresponse speed (<50 μs) are obtained, indicating well-behaved photo-sensing behaviors. The study here could offer a good reference for the controlled growth of the relevant materials, and the achieved heterostructure will find promising applications in future integrated electronic and optoelectronic devices and systems.

INTRODUCTION

Ultrathin GaTe semiconductors have attracted considerable attention due to their wonderful electrical and optoelectronic properties and are expected to be promising materials for high-sensitive photodetectors (Zolyomi et al., 2013; Lin et al., 2018; Yuan et al., 2015; Wang et al., 2015a, 2015b). Most III-VI layered compound, such as GaS, InSe, and GaSe, shares a hexagonal phase which is thermodynamically stable and can be easily achieved with ultrathin thickness (Han et al., 2020; Yu et al., 2019; Li et al., 2020a, 2020b; Mudd et al., 2013; Cai et al., 2018). As for GaTe, it possesses a different thermodynamically stable phase, namely monoclinic layered structure, with C_2/m space group symmetry, which is very difficult to be obtained with ultrathin thickness (Cai et al., 2017; Dong et al., 2019; Cui et al., 2009). From this point of view, the experimental fabrication of hexagonal GaTe (h-GaTe) is meaningful for the decreasing of the dimension of GaTe. Previous studies have indicated that the formation energy of h-GaTe is higher than that of monoclinic-GaTe (m-GaTe), leading to that h-GaTe is a metastable phase and is hardly to be achieved (Yu et al., 2019; Cai et al., 2017). Up to now, most experimental studies on GaTe and its heterojunction are based on the monoclinic structure rather than the hexagonal phase (Wang et al., 2014, 2015a, 2015b, 2019; Liu et al., 2014; Yang et al., 2016; Yan et al., 2018; Gang et al., 2014; Fonseca et al., 2016). Unlike the phase transition of transition-metal chalcogenides (Zhang et al., 2017; Song et al., 2016; Sung et al., 2017; Cho et al., 2015; Liu et al., 2018; Yin et al., 2017; Zhou et al., 2016; Yoo et al., 2017), there is no effective strategy in realizing the phase transition of GaTe from m-phase to h-phase. It is highly desired to develop a controllable preparation method for making GaTe with high-purity hexagonal phase and to realize a high-performance photoelectric device by designing the heterostructure based on ultrathin GaTe.

Here, we demonstrate, for the first time, the controllable growth of high-quality ultrathin h-GaTe on MoS_2 templates. Theoretical studies further reveal that h-GaTe is more thermodynamically stable on MoS_2 than m-GaTe, which can be attributed to the strain stretching and formation energy reduction of h-GaTe. Microscopic and spectroscopic characterizations are employed to characterize the achieved h-GaTe/MoS_2 vertical heterostructures, indicating high crystal quality. Moreover, excellent photovoltaic and photosensing properties are observed in the h-GaTe/MoS_2 vdW heterostructure. Under illumination, photo-excited electron-hole pairs are readily separated by the large built-in electrical field formed at the GaTe-MoS_2

[1]Key Laboratory for Micro-Nano Physics and Technology of Hunan Province, College of Materials Science and Engineering, School of Physics and Electronics, Hunan University, Changsha, Hunan 410082, China

[2]Key Laboratory of Inferior Crude Oil Processing of Guangdong Provincial Higher Education Institutes, School of Chemical Engineering, Guangdong University of Petrochemical Technology, Maoming, Guangdong 525000, China

[3]Key Laboratory for Matter Microstructure and Function of Hunan Province, Key Laboratory of Low-Dimensional Quantum Structures and Quantum Control of Ministry of Education, School of Physics and Electronics, Hunan Normal University, Changsha 410081, China

[4]These authors contributed equally

[5]Lead contact

*Correspondence: zhuxiaoli@hnu.edu.cn (X.Z.), liidong@hu.edu.cn (D.L.), anlian.pan@hnu.edu.cn (A.P.)

https://doi.org/10.1016/j.isci.2021.103031

This is an open access article under the CC BY-NC-ND license (http://creativecommons.org/licenses/by-nc-nd/4.0/).

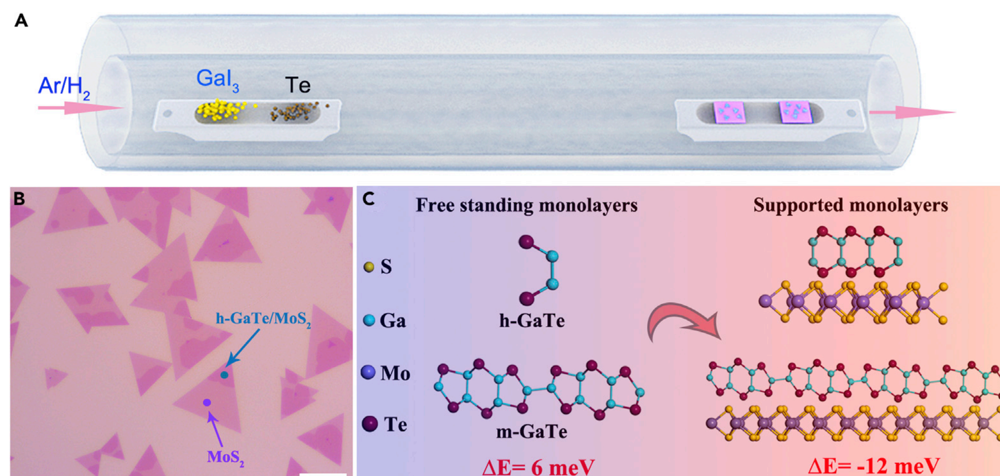

Figure 1. Synthesis of ultrathin h-GaTe on MoS_2 template via strain engineering, resulting in h-GaTe/MoS_2 heterostructures

(A) Schematic illustration of the CVD setup of ultrathin GaTe/MoS_2 heterostructure.

(B) Optical image of as-grown typical ultrathin GaTe/MoS_2 heterostructure. Scale bar, 20 μm.

(C) DFT calculations of GaTe. $\Delta E = E_h - E_m$, where E_h and E_m represent the total energy of the h-phase and m-phase per GaTe unit, respectively.

interface, leading to fast response speed (<50 μs) and high photoresponsivity (32.5 A/W). The study here could offer a good reference for the controlled growth of the relevant materials, and the obtained ultrathin GaTe/MoS_2 heterostructures will provide potential materials for application in integrated electronic and optoelectronic devices and systems.

RESULTS AND DISCUSSION

Synthesis of ultrathin h-GaTe on MoS_2 templates

Figure 1A shows the schematic diagram of the synthesis of h-GaTe/MoS_2 vertical heterostructure. During the growth process of h-GaTe/MoS_2 heterostructure, MoS_2 was first synthesized on the SiO_2/Si substrate via the typical chemical vapor deposition (CVD) growth strategy, and then, h-GaTe was fabricated on the as-achieved MoS_2 template. The monolayer GaTe is the configuration of Te–Ga–Ga–Te repeating units (in Figure S1). The detailed descriptions of the growth procedures are presented in the experimental method. Figure 1B exhibits the large-scale microscope image of the achieved samples, where partially covered ultrathin h-GaTe/MoS_2 vertical heterostructures are uniformly distributed on the substrate. Density-functional theory (DFT) calculations were further conducted to reveal the growth thermodynamics in h-GaTe/MoS_2 heterostructures (Sánchez-Royo et al., 2002; Leao and Lordi, 2011; Rahmlow et al., 2007; Kresse and Furthmüller, 1996; Blöchl, 1994; Kresse and Joubert, 1999; Klimeš et al., 2011). The relative stability between the h-phase and the m-phase is related to the formation energy difference between them. Considering the two phases have different the total numbers of atoms in their unit cells, we define $\Delta E = E_h - E_m$, where ΔE is the total energy difference per GaTe unit. As shown in Figure 1C, ΔE is about 6 meV for the free-standing condition, that is, the h-GaTe monolayer is less stable than the m-GaTe monolayer in this case, which is in accordance with the case for the bulk GaTe. On the contrary, while MoS_2 is introduced as the substrate, ΔE is reduced to −12 meV, suggesting that the h-phase is more energetically favorable than the m-phase. Generally, a substrate may impose strain and form bonding to the overlayer. However, in our model, given that both the overlayer and substrate are semiconducting and the interactions between them are vdW forces, the bonding effect is expected to be weak, and the strain should be the main reason that changes the ΔE. The interface structure for the h-phase GaTe consists of a $\sqrt{7} \times \sqrt{7}$ supercell of GaTe and a $2\sqrt{3} \times 2\sqrt{3}$ supercell of MoS_2, which gives rise to a lattice mismatch of about 0.9% between the two constituents. For the m-phase, a rectangular supercell that contains sixteen unit cells of the monoclinic GaTe monolayer and ninety unit cells of the MoS_2 monolayer is built for GaTe/MoS_2, where the lattice mismatch of 0.5% is measured. It means that the MoS_2 can definitely induce strain in the upper GaTe and influence its stability, leading to the synthesis of h-GaTe. Table S1 gives the calculated formation energy of E_h and E_m for both freestanding and supported cases.

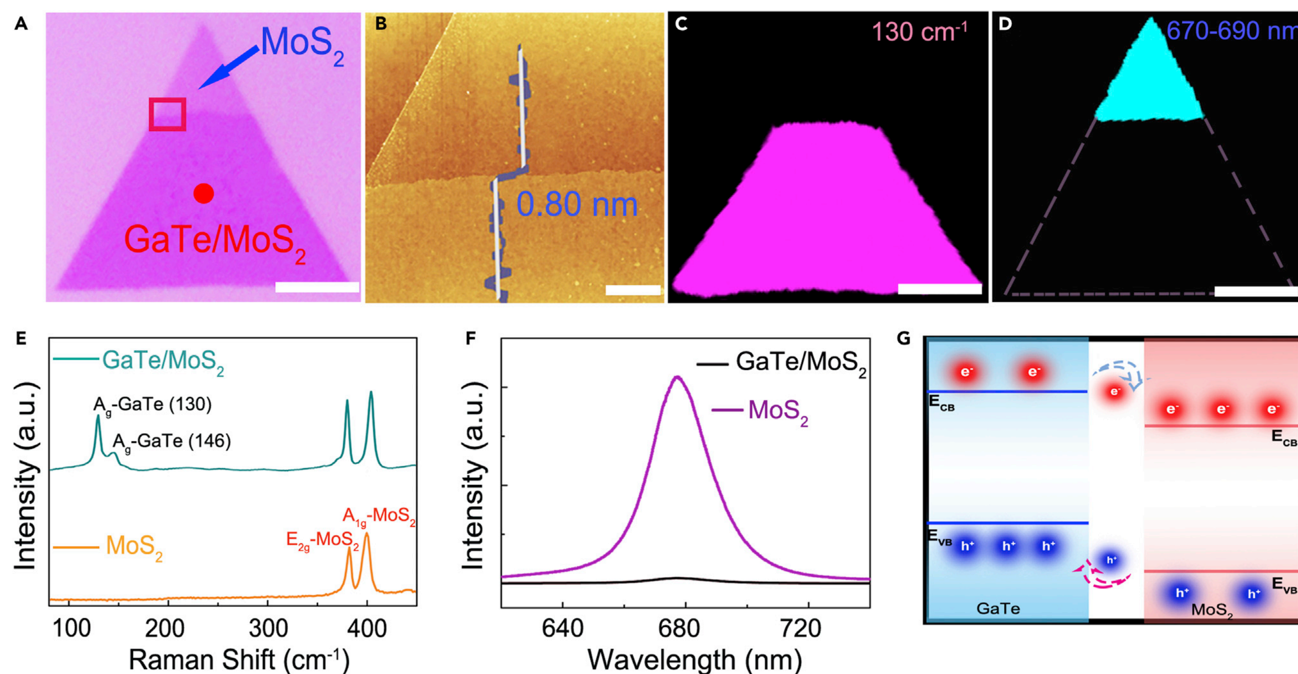

Figure 2. Optical characterization of vertically stacked GaTe/MoS_2 heterostructures

(A) Optical image of a vertical stacked GaTe/MoS_2 heterostructure. Scale bar, 20 μm.

(B) AFM image of the GaTe/MoS_2 heterostructure. Scale bar, 2 μm.

(C and D) Raman and PL mapping of the heterostructure. Scale bar, 20 μm.

(E and F) Normalized Raman and PL spectra recorded from pure materials and the heterostructure.

(G) The band alignment of the GaTe-MoS_2 heterostructure.

Optical characterization of ultrathin h-GaTe/MoS_2 vertical heterostructures

Raman and photoluminescence (PL) spectra were performed to investigate the chemical composition distributions and the local optical properties of the GaTe/MoS_2 heterostructures. Figure 2A shows a typical as-grown GaTe/MoS_2 sample with partially covered structures, where the components can be clearly identified from the optical contrast. Then, we performed thickness identification of the selected red area shown in Figure 2A, and the corresponding Atomic Force Microscope (AFM) image is depicted in Figure 2B. It indicates that the thickness of the top GaTe is about 0.8 nm, indicating the monolayer nature of h-GaTe. Figure 2C shows the spatial-resolved Raman intensity mapping at 130 cm^{-1} of the sample in Figure 2A, where strong Raman signal is collected at the lower part of the sample, corresponding to the A_{1g} mode of h-GaTe. We also collected the Raman spectra at the lower part of the sample, and the result is shown in Figure 2E, where the Raman peaks of both MoS_2 and GaTe are clearly observed, indicating the formation of h-GaTe/MoS_2 heterostructure (the monoclinic version of the Raman scattering as comparison in Figure S2 of the supplemental information). Room temperature PL mapping (670 nm–690 nm) and PL spectra are further collected and shown in Figures 2D and 2F, respectively. The weak PL emission signal from the section covered by GaTe is shown in Figure S3 of the supplemental information. It is clear that the uncovered MoS_2 region gives a strong PL emission, but a very weak PL signal can be collected in the MoS_2 region covered with GaTe. Such a typical PL quenching phenomenon observed in GaTe/MoS_2 can be attributed to the type-II band alignment at the interface which can efficiently separate the photoexcited electron-hole pairs (Figure 2G) (Li et al., 2018, 2019; Yang et al., 2017). All the results demonstrate that the as-grown heterostructures are of high quality without alloying.

TEM images of h-GaTe/MoS_2 heterostructure

We further used transmission electron microscopy (TEM) combined with energy-dispersive spectroscopy (EDS) to analyze the microstructure and chemical composition of the bilayer vertical h-GaTe/MoS_2 heterostructure. Figure 3A demonstrates the low-magnification TEM image of an as-transferred GaTe/MoS_2 heterostructure on Cu grid, where the heterointerface can be obviously identified from the contrast. Figure 3B

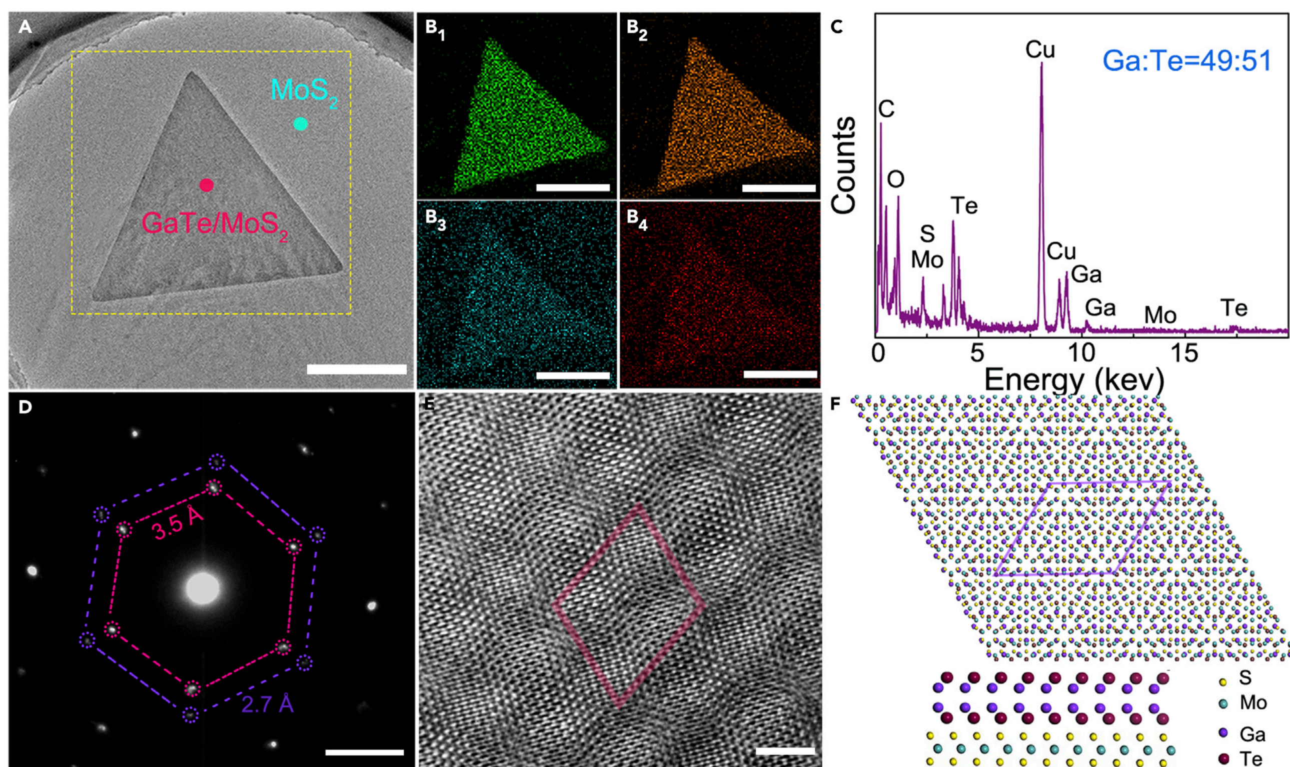

Figure 3. Atomic structure of a vertically stacked h-GaTe/MoS_2 heterostructure

(A) Low magnification TEM image of h-GaTe/MoS_2 heterostructure. Scale bar, 5 μm.

(B_1–B_4) Elements mapping of the four detected elements: Ga, Te, Mo, and S. Scale bar, 5 μm.

(C) EDS spectra collected from two different positions marked in the heterostructure.

(D) The SAED pattern of the sample taken from the overlapped region. Scale bar, 2 1/nm.

(E) HRTEM image recorded from the overlapped region. Scale bar, 2 nm.

(F) Atomic model of the h-GaTe/MoS_2 heterojunction and the supercell is marked by purple dashed line.

shows the distribution of Ga, Te, Mo, and S in the yellow rectangle region in Figure 3A. It is obvious that Mo and S are evenly distributed throughout the whole area, while Ga and Te can only be found in the triangle region. The EDS measurement is utilized to further confirm the chemical composition of the as-grown MoS_2/GaTe heterostructure. Figure 3C displays the EDS spectra recorded from the heterostructure position in Figure 3A, from which element signals of Mo, S, Ga, and Te were clearly observed. The element ratio of Ga to Te is further confirmed to be 49:51, matching well with the GaTe stoichiometric ratio. The chemical states of Ga and Te in the h-GaTe were characterized by X-ray photoelectron spectra where binding energy peaks of Ga $3d_{3/2}$, Te $3d_{3/2}$, and Te $3d_{5/2}$ are observed at 25.5 eV, 583 eV, and 54.7 eV, respectively, indicating the existence of GaTe (Figure S4). Two sets of hexagonal symmetrical diffraction spots in the same direction can be clearly identified in the selected area electron diffraction (SAED) graph in Figure 3D, corresponding to the MoS_2 lattice (2.7 Å) and h-GaTe lattice (3.5 Å), respectively. On the contrast, SAED pattern of m-GaTe is a parallelogram (Figure S5), which is totally different from that of h-GaTe. The high-resolution TEM image of the overlapped region in Figure 3E displays apparent Moire patterns, which is attributed to the overlapping lattices between GaTe and MoS_2, matching well with the atomic structure model of the GaTe/MoS_2 heterostructure in Figure 3F. All the above characterizations clearly illustrate that the as-fabricated vertical h-GaTe/MoS_2 heterostructures are of good crystal quality.

Non-linear optical properties of GaTe flakes

To study the stacking mode of h-GaTe layers, we further explored second harmonic generation (SHG) performance of h-GaTe and determined the symmetry of the sample. SHG is a nonlinear optical phenomenon, which is ultrasensitive to the centrosymmetry of 2D materials. It is noteworthy that the MoS_2 obtained in our experiment possesses 2H phase with a centrosymmetry structure, leading to weak SHG signals in bilayer

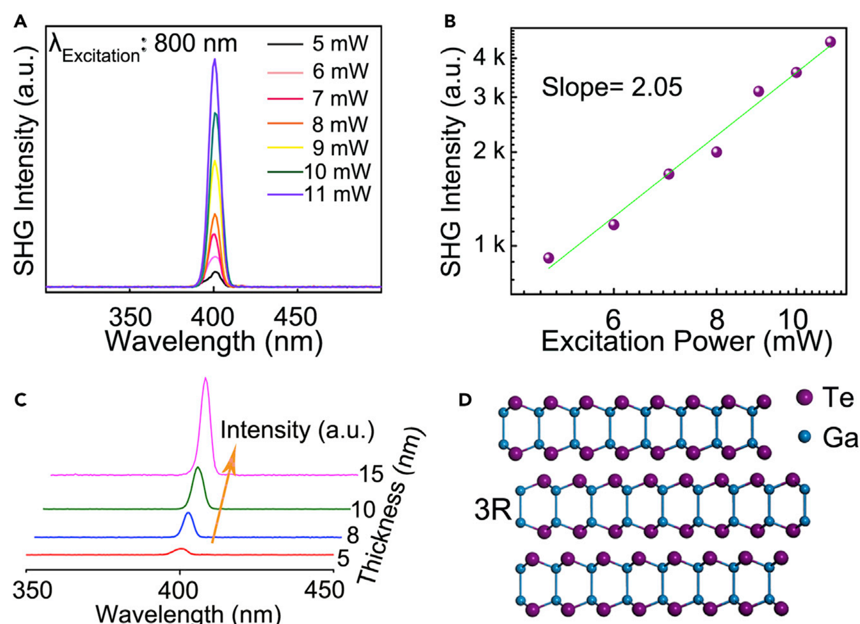

Figure 4. Non-linear optical properties of GaTe flakes

(A) The evolution of the SHG intensity of h-GaTe with incident laser power intensity.

(B) The SHG intensity shows a power law dependence on the excitation power with the coefficient fitted to 2.05.

(C) The evolution of the SHG intensity with sample thickness.

(D) The 3R stack mode of h-GaTe.

2H-MoS_2 (Figure S6). Here, a GaTe/MoS_2 heterostructure integrated with bilayer MoS_2 is choosen to investigate the SHG performance of the GaTe, and the SHG characteristics of the samples were collected with transmission geometry. As shown in Figure 4A, an expected single peak located at 400 nm is observed, which is exactly at the doubled frequency of the femtosecon (fs)-laser power of 800-nm excitation wavelength. Moreover, the SHG intensity monotonically increases with the enhancement of the fs-laser power. The detailed relationship between SHG intensity and laser power is plotted in Figure 4B, in which a slope of 2.05 can be acquired, in accordance with the theoretical value of 2, demonstrating the second-order nonlinear optical process (Zeng et al., 2019; Saynatjoki et al., 2017). We also investigate the relationship between the thickness and the SHG of the GaTe in Figure 4C. As can be seen, the SHG intensity is enhancing with the increase of sample thickness, suggesting the h-GaTe flakes are 3R stacking mode, with the atomic structure shown in Figure 4D. The results indicate that the achieved sample can be potentially used in nonlinear optics.

Photoresponse characterizations of bilayer GaTe/MoS_2 heterostructures

To further investigate the electrical charge transport properties and optoelectronic performance of the resulted ultrathin GaTe/MoS_2 vertical heterostructure, the optoelectronic devices based on the obtained bilayer GaTe/MoS_2 p-n heterojunctions were investigated schematically under vacuum at room temperature. Figure 5A exhibits the configuration of the h-GaTe/MoS_2 photodetector device, where Cr/Au electrodes are separately fabricated on monolayer MoS_2 and heterostructure region. The transport characteristics in Figure 5B demonstrate an obvious current rectification behavior with V_g from 0 to 60 V, which is common with the behaviors that are observed in traditional p-n junctions (electrodes 2 and 3). The inset image of Figure 5B displays a typical optical image of the as-fabricated bilayer p-n heterojunction device (device area: 42 μm^2). Figure S7 also shows the output characteristics under measured using difference electrodes contact from 0 to 60V. Figure 5C plots the I_{ds}-V_{ds} curves under 520-nm light irradiation with power densities changing from 0.01 to 78.5 mW/cm^2 at zero gate bias. Obviously, the photocurrent increases gradually with the increase of light power intensity. From the magnified I_{ds}-V_{ds} curves shown in Figure 5D, apparent photovoltaic behaviors are observed with maximum open-circuit voltage reaching up to 0.145 V at a power density of 78.5 mW/cm^2. Figure 5E displays the extracted short-circuit current (I_{sc}) and open-circuit voltage (V_{oc}) as a function of incident light power density. It is obvious that both I_{sc} and V_{oc}

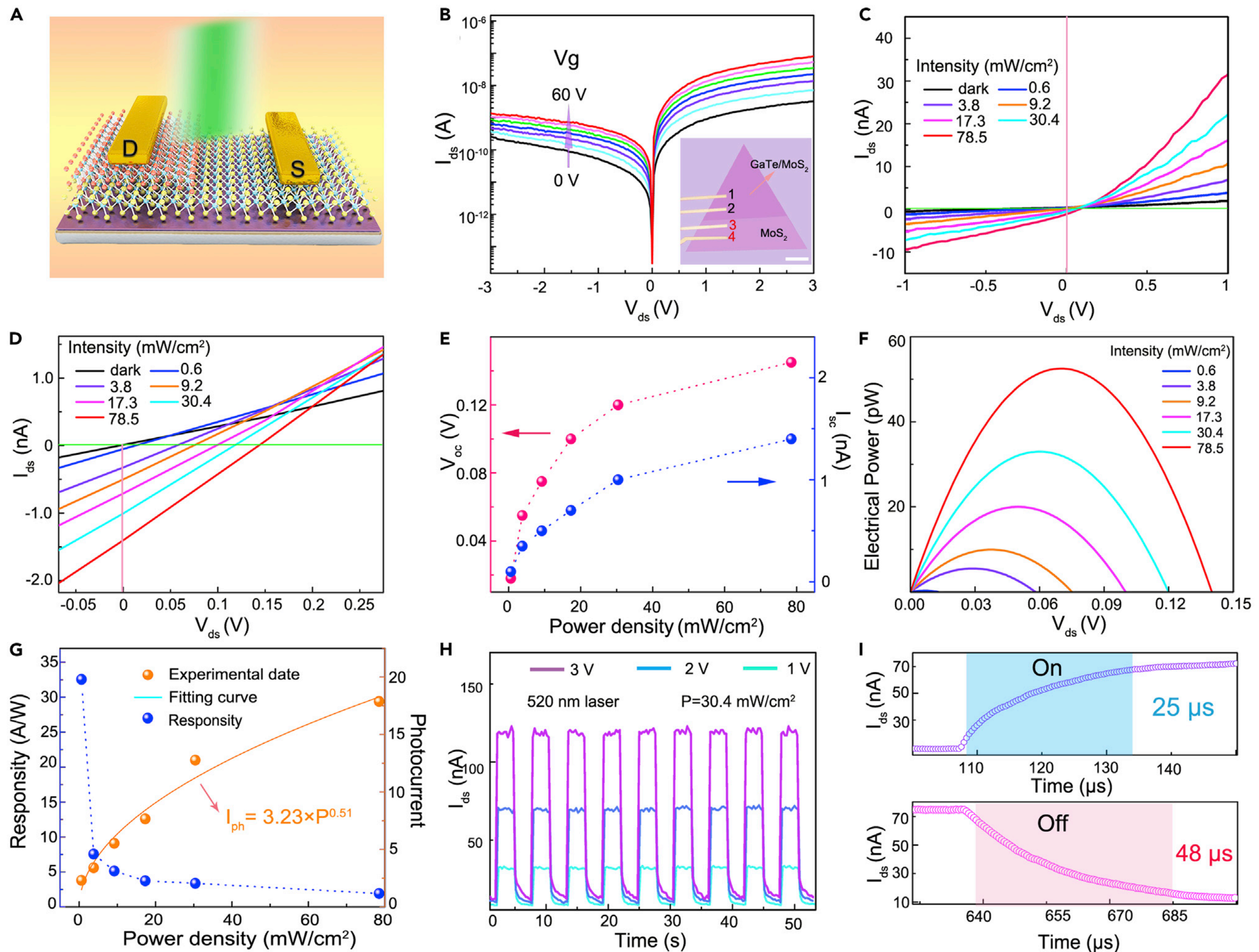

Figure 5. Photoresponse characterizations of bilayer GaTe/MoS_2 heterostructures

(A) Device schematic diagram of the vertically stacked GaTe/MoS_2 p-n heterojunction.

(B) I_{ds}-V_{ds} characteristic of the p-n heterojunction in the dark condition. Inset: optical image of the device. Scale bar, 5 μm.

(C and D) I_{ds}-V_{ds} curves across the p-n junction measured with different incident power densities.

(E) The short-circuit currents and open-circuit voltages as a function of light power density.

(F) Electrical power under various light illumination power densities.

(G) Dependence of photocurrent and responsivity on illumination power densities.

(H) Photoswitching characterization of the device under different bias voltage.

(I) Response speed of the device.

increase gradually with the increase of the incident light power density. Figure 5F plots the curves as a function of the V_{ds} under different light power density. The generated electrical power (P_{EL}) in the p-n diode can further be calculated with equation $P_{EL} = I_{ds} \times V_{ds}$. It suggests that the maximum P_{EL} is generated at 0.075 V with a light intensity of 78.5 mW/cm^2. It also means that the most suitable output working voltage is 0.075 V for a photovoltaic device. The photocurrent at V_{ds} = 1 V is extracted and plotted in Figure 5G, where the photocurrent (I_{ph}) is defined as $I_{ph} = I_{light}$-I_{dark}. The relationship between photocurrent and laser power density can be fitted within an equation of $I_{ph} = aP^{\alpha}$, where a is the parameter related to the photodetector responsivity, P is the laser power density, and α is dimensionless exponent of the power law. The parameters a and α are determined to be 3.2 and 0.51, respectively. The responsivity (R) can be calculated with the equation of $R = I_{ph}/PA$, where A is the effective area of the device channel. Benefiting from the ultrathin structure and the large built-in electrical field at the junction interface, the photo-generated electron-hole pairs can be effectively separated, resulting in high responsivity (Li et al., 2017). The maximum photoresponsivity is measured to be 32.5 A/W at an incident power of 0.6 mW/cm^2, which is higher than

that of previous reports on multilayer m-GaTe/MoS_2 vertical heterostructures.[13-15, 19] Time-resolved photoresponse measurements were performed to further investigate the photoresponse speed of the h-GaTe/MoS_2 heterojunction photodetector, and the results are shown in Figure 5H. As can be seen, by periodically turning on and off the laser (520 nm, 30.4 mW/cm^2), the photocurrent can be switched well between the on and off state, showing excellent stability and reliability. Further investigation indicates that the device possesses rise time (t_{rise}) of about 25 μs and fall time (t_{decay}) of about 48 μs, which is faster than the pure GaTe and GaTe/MoS_2 vertical heterostructure-based device (Figure 5I) (Wang et al., 2014, 2015a, 2015b). Table S2 gives the comparison of the photoresponse performance of our h-GaTe/MoS_2 p-n vertical junction with several other GaTe reports. Photoswitching properties of the device illuminated by different wavelengths (520 nm and 800 nm) are further carried out in Figure S8, where stable photoresponse at each wavelength is observed. Although the photocurrent illuminated by the 800-nm laser is weak than the 520-nm laser, it is surprising that the device can respond not only to visible light but also to near-infrared (NIR) light. The light response to NIR light may be originated from the interlayer excitation, which is beyond both the MoS_2 and the GaTe absorption edge.

Conclusions

In summary, we demonstrate the successful synthesis of high-quality ultrathin h-GaTe/MoS_2 heterostructures. Theoretical calculation studies reveal that the achieved h-GaTe is more stable on 2D MoS_2 substrate than m-GaTe, which leads to greater strain stretching and reduces the formation energy of h-GaTe. Excellent photovoltaic and photosensing properties are observed in the ultrathin p-n GaTe/MoS_2 heterojunctions. With the drain bias voltage fixed at 1 V, high photoresponsivity of 32.5 A/W has been realized at light of 520 nm. Furthermore, ultra-fast response times t_{rise} (25 μs) and t_{decay} (48 μs) are also proven. The study here could offer a good reference for the controlled growth of the relevant materials, and the achieved GaTe/MoS_2 heterostructure will find promising applications in future integrated electronic and optoelectronic devices and systems.

Limitations of the study

In addition to the ultrathin h-GaTe being prepared on MoS_2 templates in this study, more relevant phase transition materials can be prepared and applied for more breakthroughs in structure control and performance enhancement. Considering the limitation of the experiment platform, the detailed process of in situ phase transition remains unknown.

STAR★METHODS

Detailed methods are provided in the online version of this paper and include the following:

- KEY RESOURCES TABLE
- RESOURCE AVAILABILITY
  - Lead contact
  - Materials availability
  - Date and code availability
- METHOD DETAILS
  - Synthesis of the 2D h-GaTe/MoS_2 heterostructure
  - Characterization
  - Density functional theory calculations
- QUANTIFICATION AND STATISTICAL ANALYSIS

SUPPLEMENTAL INFORMATION

Supplemental information can be found online at https://doi.org/10.1016/j.isci.2021.103031.

ACKNOWLEDGMENTS

The authors are grateful to the National Natural Science Foundation of China (Nos. 51902098, U19A2090, 62090035, 51972105, 51525202, 61574054, 11774084, and 91833302), the Hunan Provincial Natural Science Foundation of China (No. 2018RS3051), the Key Program of Science and Technology Department of Hunan Provice (2019XK2001 and 2020XK2001), Hunan Provincial (China) Natural Science Foundation for Excellent Young Scholars (No. 2021JJ20016), and the Projects of PhDs' Start-up Research of GDUPT (No. 72100003175) and the Project of Educational Commission of Hunan Province of China (No. 18A003).

AUTHOR CONTRIBUTIONS

F.L., X.Z., D.L., and A.P. designed the research idea and experiments. M.C. carried out DFT calculation. Y.W., X.Z., Z.Z., D.Z., J.Y., and Z.L. analyzed the date. All authors discussed the results and commented on the manuscript.

DECLARATION OF INTERESTS

The authors declare no competing financial interest.

Received: March 27, 2021
Revised: June 15, 2021
Accepted: August 20, 2021
Published: September 24, 2021

REFERENCES

Blöchl, P. (1994). Projector augmented-wave method. Phys. Rev. B *50*, 17953.

Cai, H., Chen, B., Wang, G., Soignard, E., Khosravi, A., Manca, M., Marie, X., Chang, S., Urbaszek, B., and Tongay, S. (2017). Synthesis of highly anisotropic semiconducting GaTe nanomaterials and emerging properties enabled by epitaxy. Adv. Mater. *29*, 1605551.

Cai, H., Chen, B., Blei, M., Chang, S., Wu, K., Zhuang, H., and Tongay, S. (2018). Abnormal band bowing effects in phase instability crossover region of GaSe1-xTex nanomaterials. Nat. Commun. *9*, 1927.

Cho, S., Kim, S., Kim, J., Zhao, J., Seok, J., Keum, D., Baik, J., Choe, D., Chang, K., Suenaga, K., et al. (2015). Phase patterning for ohmic homojunction contact in $MoTe_2$. Science *349*, 625–628.

Cui, Y., Caudel, D., Bhattacharya, P., Burger, A., Mandal, C., Johnstone, D., and Payne, S. (2009). Deep levels in GaTe and GaTe:In crystals investigated by deep-Level transient spectroscopy and photoluminescence. J. Appl. Phys. *105*, 053709.

Dong, J., Gradwohl, K., Xu, Y., Wang, T., Zhang, B., Xiao, B., Teichert, C., and Terahertz, W. (2019). Terahertz emission from layered GaTe crystal due to surface lattice reorganization and in-plane noncubic mobility anisotropy. Photon. Res. *7*, 518.

Fonseca, J., Tongay, S., Topsakal, M., Chew, A., Lin, A., Ko, C., Luce, A., Salleo, A., Wu, J., and Dubon, D. (2016). Bandgap restructuring of the layered semiconductor gallium telluride in air. Adv. Mater. *28*, 6465–6470.

Gang, Y., Liu, Z., Xie, X., Yang, X., and Shen, G. (2014). Flexible photodetectors with single-crystalline GaTe nanowires. J. Mater. Chem. C. *2*, 6104–6110.

Han, W., Li, C., Yang, S., Luo, P., Wang, F., Feng, X., Liu, K., Pei, K., Li, Y., Li, H., et al. (2020). Atomically thin Oxyhalide solar-blind UV photodetectors. Small *16*, 2000228.

Klimeš, J., Bowler, D., and Michaelides, A. (2011). Van der Waals density functionals applied to solids. Phys. Rev. B. *83*, 195131.

Kresse, G., and Furthmüller, J. (1996). Efficiency of ab-initio total energy calculations for metals and semiconductors using a plane-wave basis set. Comput. Mater. Sci. *6*, 15.

Kresse, G., and Joubert, D. (1999). From ultrasoft pseudopotentials to the projector augmented-wave method. Phys. Rev. B. *59*, 1758.

Leao, C., and Lordi, V. (2011). Ab initio guided optimization of GaTe for radiation detection applications. Phys. Rev. B. *84*, 165206.

Li, D., Chen, M., Sun, Z., Yu, P., Liu, Z., Ajayan, P., and Zhang, Z. (2017). Two-dimensional non-volatile programmable p-n junctions. Nat. Nanotechnol. *12*, 901–906.

Li, H., Liu, H., Zhou, L., Wu, X., Pan, Y., Ji, W., Zheng, B., Zhang, Q., Zhuang, X., Zhu, X., et al. (2018). Strain-tuning atomic substitution in two-dimensional atomic crystals. ACS Nano *12*, 4853–4860.

Li, F., Feng, Y., Li, Z., Ma, C., Qu, J., Wu, X., Li, D., Zhang, X., Yang, T., He, Y., et al. (2019). Rational kinetics control toward universal growth of 2D vertically stacked heterostructures. Adv. Mater. *31*, 1901351.

Li, D., Zhu, C., Liu, H., Sun, X., and Pan, A. (2020a). Light-triggered two-dimensional lateral homogeneous p-n diodes for opto-electrical interconnection circuits. Sci. Bull. *65*, 293–299.

Li, F., Xu, B., Yang, W., Qi, Z., Ma, C., Wang, Y., Zhang, X., Luo, Z., Liang, D., Li, D., et al. (2020b). High-performance optoelectronic devices based on Van der Waals vertical $MoS_2/MoSe_2$ heterostructures. Nano Res. *13*, 1053–1059.

Lin, Z., Liu, Y., Halim, U., Ding, M., Liu, Y., Wang, Y., Jia, C., Chen, P., Duan, X., Wang, C., et al. (2018). Solution-processable 2D semiconductors for high-performance large-area electronics. Nature *562*, 254–258.

Liu, F., Shimotani, H., Shang, H., Kanagasekaran, T., Zolyomi, V., Drummond, N., Falko, V., and Tanigaki, K. (2014). High-sensitivity photodetectors based on multilayer GaTe flakes. ACS Nano *8*, 752–760.

Liu, L., Wu, J., Wu, L., Ye, M., Liu, X., Wang, Q., Hou, S., Lu, P., Sun, L., Zheng, J., et al. (2018). Phase-selective synthesis of 1T′ MoS_2 monolayers and heterophase bilayers. Nat. Mater. *17*, 1108–1114.

Mudd, G., Svatek, S., Ren, T., Patanè, A., Makarovsky, O., Eaves, L., Beton, P., Kovalyuk, Z., Lashkarev, G., Kudrynskyi, Z., et al. (2013). Tuning the bandgap of exfoliated InSe nanosheets by quantum confinement. Adv. Mater. *25*, 5714–5718.

Rahmlow, D., Depoy, D., Fourspring, P., Ehsani, H., Lazowasem, J., and Gratrix, E. (2007). Development of front surface, spectral control filters with greater temperature stability for thermophotovoltaic energy conversion. AIP Conf. Proc. *890*, 59.

Sánchez-Royo, J., Pellicer-Porres, J., Segura, A., Muñoz-Sanjosé, V., Tobías, G., Ordejón, P., Canadell, E., and Huttel, Y. (2002). Angle-resolved photoemission study and first-principles calculation of the electronic structure of GaTe. Phys. Rev. B *65*, 115201.

Saynatjoki, A., Karvonen, L., Rostami, H., Autere, A., Mehravar, S., Lombardo, A., Norwood, R., Hasan, T., Peyghambarian, N., Lipsanen, H., et al. (2017). Ultra-strong nonlinear optical processes and trigonal warping in MoS_2 layers. Nat. Commun. *8*, 893.

Song, S., Keum, D., Cho, S., Perello, D., Kim, Y., and Lee, Y. (2016). Room temperature semiconductor−metal transition of $MoTe_2$ thin films engineered by strain. Nano Lett. *16*, 188–193.

Sung, J., Heo, H., Si, S., Kim, Y., Noh, H., Song, K., Kim, J., Lee, C., Seo, S., Kim, D., et al. (2017). Coplanar semiconductor–metal circuitry defifined on few-layer $MoTe_2$ via polymorphic heteroepitaxy. Nat. Nanotechnol. *12*, 1064–1070.

Wang, Z., Xu, K., Li, Y., Zhan, X., Safdar, M., Wang, Q., Wang, F., and He, J. (2014). Role of Ga vacancy on a multilayer GaTe phototransistor. ACS Nano *8*, 4859–4865.

Wang, Z., Safdar, M., Mirza, M., Xu, K., Wang, Q., Huang, Y., Wang, F., and He, J. (2015a). High-performance flexible photodetectors based on GaTe nanosheets. Nanoscale *7*, 7252–7258.

Wang, F., Wang, Z., Xu, K., Wang, F., Wang, Q., Huang, Y., Yin, L., and He, J. (2015b). Tunable GaTe-MoS_2 van der Waals p−n junctions with novel optoelectronic performance. Nano Lett. *15*, 7558–7566.

CellPress
OPEN ACCESS

Wang, H., Chen, M., Zhu, M., Wang, Y., Dong, B., Sun, X., Zhang, X., Cao, S., Li, X., Huang, J., et al. (2019). Gate tunable giant anisotropic resistance in ultra-thin GaTe. Nat. Commun. *10*, 2302.

Yan, X., Zhang, D., Liu, C., Bao, W., Wang, S., Ding, S., Zheng, G., and Zhou, P. (2018). High performance amplifier element realization via MoS_2/GaTe heterostructures. Adv. Sci. *5*, 1700830–1700836.

Yang, S., Wang, C., Ataca, C., Li, Y., Chen, H., Suslu, A., Grossman, J., Jiang, C., Liu, Q., and Tongay, S. (2016). Self-driven photodetector and ambipolar transistor in atomically thin GaTe-MoS_2 p−n vdW heterostructure. ACS Appl. Mater. Interfaces *8*, 2533–2539.

Yang, T., Zheng, B., Wang, Z., Yang, T., Zheng, B., Wang, Z., Xu, T., Pan, C., Zou, J., Zhang, X., et al. (2017). Van der Waals epitaxial growth and optoelectronics of large-scale WSe_2/SnS_2 vertical bilayer p–n junctions. Nat. Commun. *8*, 1906.

Yin, Y., Miao, P., Zhang, Y., Han, J., Zhang, X., Gong, Y., Gu, L., Xu, C., Yao, T., Xu, P., et al. (2017). Significantly increased Raman enhancement on MoX_2 (X = S, Se) monolayers upon phase transition. Adv. Funct. Mater. *16*, 1606694.

Yoo, Y., DeGregorio, Z., Su, Y., Koester, S., and Johns, J. (2017). In-plane 2H-1T' $MoTe_2$ homojunctions synthesized by flux-controlled phase engineering. Adv. Mater. *29*, 1605461.

Yu, Y., Ran, M., Zhou, S., Wang, R., Zhou, F., Li, H., Gan, L., Zhu, M., and Zhai, T. (2019). Phase-Engineered synthesis of ultrathin hexagonal and monoclinic GaTe flakes and phase transition study. Adv. Funct. Mater. *29*, 1901012.

Yuan, X., Tang, L., Wang, P., Chen, Z., Zou, Y., Su, X., Zhang, C., Liu, Y., Wang, W., Liu, C., et al. (2015). Wafer-scale arrayed p-n junctions based on few-layer epitaxial GaTe. Nano Res. *8*, 3332.

Zeng, Z., Sun, X., Zhang, D., Zheng, W., Fan, X., He, M., Xu, T., Sun, L., Wang, X., and Pan, A. (2019). Controlled vapor growth and nonlinear optical applications of large area 3R phase WS_2 and WSe_2 atomic layers. Adv. Funct. Mater. *29*, 1806874.

Zhang, Q., Xiao, Y., Zhang, T., Weng, Z., Zeng, M., Yue, S., Mendes, R., Wang, L., Chen, S., Rummeli, M., et al. (2017). Iodine-mediated chemical vapor deposition growth of metastable transition metal dichalcogenides. Chem. Mater. *29*, 4641–4644.

Zhou, L., Zubair, A., Wang, Z., Zhang, X., Ouyang, F., Xu, K., Fang, W., Ueno, K., Li, J., and Palacios, T. (2016). Synthesis of high-quality largearea homogenous 1T' MoTe2 from chemical vapor deposition. Adv. Mater. *28*, 9526–9531.

Zolyomi, Z., Drummond, N., and Faiko, V. (2013). Band structure and optical transitions in atomic layers of hexagonal gallium chalcogenides. Phys. Rev. B *87*, 195403.

STAR★METHODS

KEY RESOURCES TABLE

REAGENT or RESOURCE	SOURCE	IDENTIFIER
Chemicals, peptides, and recombinant proteins		
Gallium(III) iodide	Alfa Aesar	CAS: 13450-91-4
Tellurium powder	Alfa Aesar	CAS: 13494-80-9
Sulfur powder	Alfa Aesar	CAS: 7704-34-9
Molybdenum(VI) oxide	Alfa Aesar	CAS: 1313-27-5
sodium chloride	Alfa Aesar	CAS: 7647-14-5
Software and algorithms		
Origin 8.1	OriginLab	https://www.originlab.com/

RESOURCE AVAILABILITY

Lead contact

Further information and requests for resources and materials should be directed to and will be fulfilled by the Lead Contact, Prof. Anlian Pan (anlian.pan@hnu.edu.cn).

Materials availability

This study did not generate new unique reagents.

Date and code availability

- Data reported in this paper will be shared by the lead contact upon request.
- This paper does not report original code.
- Any additional information required to reanalyze the data reported in this paper is available from the lead contact upon request.

METHOD DETAILS

Synthesis of the 2D h-GaTe/MoS_2 heterostructure

The GaTe/MoS_2 heterostructures were synthesized by a two-step growth method using CVD technology. The first-step growth of monolayer MoS_2 is a traditional process. The mixed powder of 0.5mg sodium chloride (NaCl) and 2 mg Molybdenum(VI) oxide (MoO_3) was selected as the solid source for the first-step growth. For vertical GaTe/MoS_2 heterostructures, as-grown MoS_2 templates were placed at the downstream of a CVD system. The temperature was gradually heated up to 690°C in 20 min, and then kept the temperature for 5 min. Meanwhile, the 5mg Te powder was put in the upstream region about 450°C and the 2mg GaI_3 powder was put in the low temperature region about 210°C. A mixture flow of 100 sccm Ar/H_2 (with 10% H_2) was operated as the carrier gas. After the growth process, the furnace was cooled down to room temperature.

Characterization

The optical images of heterostructures were characterized using optical microscopy (Zeiss Axio Scope A1). The optical measurements (PL and Raman) were performed with the confocal-PL system (WITec, alpha-300). A 520 nm solid state laser (power: about 5 mW, spot size: 1–2 μm) was used to excite the samples. For atomic-structural characterizations measurements, The STEM and EDS measurements were carried out on JEOL ARM200F microscope operated at 200 kV and equipped with a probe-forming aberration corrector. Standard e-beam lithography (EBL, Raith 150) and metal thermal evaporation were performed to fabricate the Au/Cr (10 nm/50 nm) electrodes on the produced heterostructures. The electrical and optoelectronic properties of the heterostructures were measured in vacuum with Lake Shore Probe Station and Agilent B1500A semiconductor analyzer at room temperature.

CellPress
OPEN ACCESS

Density functional theory calculations

DFT calculations were performed using the Vienna Ab Initio Simulation Package. The pseudopotentials were constructed by the projector augmented wave method. Van der Waals dispersion (vdW) forces between the GaTe monolayer and MoS_2 substrate were accounted for through the opt PBE-vdW functional by using the vdW-DF method. A 12 × 12 Monkhorst-Pack k-mesh was used to sample the surface Brillouin zone (BZ) for the hexagonal phase and a 6 × 6 k-mesh was use for the monoclinic phase. For the interface structure, i.e., GaTe/MoS_2, a 6 × 6 was used for the hexagonal phase (Table S1). While for the monoclinic phase, a 1 × 3 k-mesh was used. A plane-wave energy cutoff of 300 eV was used for structural relaxation and total energy calculations.

QUANTIFICATION AND STATISTICAL ANALYSIS

Each value of SHG intensity shown in Figure 4B of the main manuscript corresponds to the average value obtained from multiple measurements at a given excitation power.